



Derivation of crack bridging stresses in engineered cementitious composites under combined opening and shear displacements



Chang Wu^{a,*}, Christopher K.Y. Leung^a, Victor C. Li^b

^a Department of Civil and Environmental Engineering, The Hong Kong University of Science and Technology, Hong Kong, China

^b Department of Civil and Environmental Engineering, University of Michigan, Ann Arbor, USA

ARTICLE INFO

Keywords:

Engineered cementitious composites
Fiber reinforcement (E)
Modeling (E)
Micromechanics (C)
Characterization (B)

ABSTRACT

The mechanical behavior of Engineered Cementitious Composites (ECC) is strongly dependent on the bridging of cracks by fibers. Due to the bridging action of fibers, tensile and shear stresses can be transferred through cracks in ECC members. In this study, a micromechanics based theoretical model is proposed to describe the shear transfer mechanism on the crack surface due to fiber bridging effect. The model focuses on flexible fibers and both the normal stress along the crack opening direction and the shear stress transferred across the crack surfaces are derived under the coupled effect of crack opening displacement (COD) and shear sliding. With the proposed model, the mechanism of fibers contributing to the shear transfer can be understood and the effect of various micromechanical parameters can be investigated. The simulation results can provide insight on the behavior of ECC under shear loading when cracks are propagating under mixed mode.

1. Introduction

To overcome the brittleness of concrete and the difficulty to control the formation and opening of cracks, various approaches to reinforcing cementitious composites with fibers have been made. Specifically, High Performance Fiber-Reinforced Cementitious Composites (HPFRCC), which is highly ductile material exhibiting multiple cracks and strain-hardening characteristics under uniaxial tensile stress, has been developed and gained ground in research and application [1–3]. As a class of HPFRCC, Engineered Cementitious Composites (ECC) is designed according to basic principles of micromechanics and fracture mechanics [4–6]. Prepared with cement, mineral admixture, fine aggregates (maximum grain size is usually 0.15 mm), water, superplasticizer and < 2% volume of short fibers, the ultimate tensile strength of ECC can reach over 3%, while the opening of each crack is usually controlled to be < 60 μm [7–9].

Due to its ultra-high tensile durability and energy dissipation capacity, ECC is being considered for replacing conventional concrete in structures in high-intensity earthquake regions [10]. The shear behavior of ECC members has therefore attracted the attentions of many researchers and designers. While obvious improvement in performance has been demonstrated by various experiments on shear critical specimens [11–21], most investigations on the behavior of shear-critical ECC structural members are experimental in nature and limited in modeling aspects. In a number of studies [22–24], models for predicting the shear

behavior of ECC members have been proposed, but all of these models are modified from models for concrete according to empirical test data. Without considering the effects of fiber, matrix and interface on the fundamental crack bridging mechanisms, these models are limited in accuracy and applicability to general cases.

The highly improved tensile ductility of ECC compared with ordinary concrete is achieved by the crack bridging effect of fibers. Moreover, due to the fiber bridging effect, tensile and shear stresses can be transferred through multiple cracks in ECC members. As a fundamental mechanism governing the behavior of cracked ECC members under shear loading, the shear transfer mechanism of fibers on the crack surface must be properly understood. While crack fiber bridging behavior of ECC under direct tension has been widely studied [4,8,25], little attention has been paid to the effect of fibers on the shear transfer behavior of cracked ECC. Several experimental studies have been conducted on this issue [21,26], but theoretical models considering the fiber bridging action for quantitatively evaluating the shear transfer capacity of cracked ECC are rather rare. Kabele [27,28] built a multi-scale framework for modeling structural performance of HPFRCC, in which analytical models for simulating the bridging stresses of a fiber-bridged crack under opening and sliding are outlined from microscale to mesoscale. However, the model did not consider two-way fiber pullout which is a commonly observed mechanism in ECC. Also, the modeling of matrix spalling is relatively basic as the occurrence of spalling is assumed to be governed by an arbitrary fiber inclination

* Corresponding author.

E-mail addresses: changwu@ust.hk (C. Wu), ckleung@ust.hk (C.K.Y. Leung), vcli@umich.edu (V.C. Li).

angle.

This paper aims at establishing a micromechanics-based theoretical model to describe the shear transfer mechanism on the crack surface of ECC with respect to the fiber bridging action. Following the framework outlined by Kabele [27,28] and focusing on cementitious composites reinforced with flexible fibers, both the normal stress along the crack opening direction and the shear stress transferred parallel to the crack surfaces are derived under the coupled effect of crack opening displacement (COD) and shear sliding. The fiber snubbing effect and strength reduction of inclined fibers, fiber rupture, matrix spalling as well as two-way fiber pullout mechanism are considered. With the proposed model, the behavior of a single crack in ECC under mixed crack mode is analyzed and discussed. The effects of various micro-mechanical parameters on the shear transfer behavior on the crack surface of ECC are investigated. The simulation results can provide insight on the behavior of ECC under shear loading when cracks are propagating under mixed mode. It is expected that the proposed model will provide useful fundamental understanding for the further development of a rational model for predicting the shear behavior of ECC members.

2. Modeling of single fiber behavior under combined opening and sliding

2.1. Modeling of single fiber pullout behavior

Prior to establishing a model for simulating the crack bridging behavior, the single fiber pullout behavior against the surrounding matrix should be first investigated. Single fiber pullout tests [5,8] indicate that two stages can be observed when a fiber embedded in matrix is subjected to a pullout force, and they are: (1) debonding stage and (2) pullout stage. The debonding process can be simulated as the propagation of a tunneling crack along the interface between fiber and matrix. The pullout stage begins after complete debonding of the interface which is usually accompanied by a load drop. In the debonding stage, the behavior of the interface is controlled by both chemical bond and frictional bond; while in the pullout stage the behavior of the interface is fully governed by the frictional bond [8,25]. The pullout force (P) versus pullout displacement (u) relation of an aligned fiber with a certain embedded length (L_e) was theoretically derived by Lin et al. [25] as:

$$P(u) = \begin{cases} \pi \sqrt{\frac{1}{2} E_f d_f^3 (\tau_0 u + G_d) (1 + \eta)} & (0 \leq u \leq u_0) \quad (a) \\ \pi \tau_0 (L_e - u + u_0) [d_f + \beta(u - u_0)] & (u_0 < u \leq L_e) \quad (b) \end{cases} \quad (1)$$

in which, E_f and d_f are Young's modulus and diameter of the fiber, respectively, and η is a parameter representing the ratio of effective stiffness between fiber and matrix. Eq. 1 can fully describe the single fiber pullout behavior by assuming constant frictional bond (τ_0) and chemical bond (G_d) of the interface at the debonding stage (Eq. 1(a)), and by setting a coefficient β to consider the slip-hardening/softening effect during the pullout stage (Eq. 1(b)). The same P - δ relation is applied in the present study. The critical displacement (u_0) at which the fiber is completely debonded is given by:

$$u_0 = \frac{2\tau_0 L_e^2 (1 + \eta)}{E_f d_f} + \frac{L_e}{E_f} \sqrt{\frac{8G_d E_f (1 + \eta)}{d_f}} \quad (2)$$

For randomly distributed short fiber reinforced cementitious composites, most of the fibers are not oriented normal to the crack plane. When a randomly oriented fiber is subjected to a pullout force due to pure opening of a crack as shown in Fig. 1(a), the fiber bridging force will increase due to the “snubbing effect” [29]. The pullout load for an inclined fiber ($P(\phi)$) is then related to the pullout force of an aligned fiber ($P(0)$) through the following equation, assuming the fiber to

change direction over a frictional pulley [4,30,31].

$$P(\phi) = P(0)e^{f\phi} \quad (3)$$

In Eq. 3, the parameter f is defined as snubbing coefficient.

2.2. Consideration of shear sliding

When the two surfaces of the crack shown in Fig. 1(a) begin to undergo relative sliding, the fiber bridging the two crack surfaces will be pulled out further and the part of fiber between the crack surfaces will rotate by an angle as shown in Fig. 1(b). At a given crack opening displacement (COD), ω , and sliding, Δ , the rotating angle γ and the actual pullout length δ are related by the following equations:

$$\gamma = \arctan\left(\frac{\Delta}{\omega}\right) \quad (4)$$

$$\delta = \sqrt{\Delta^2 + \omega^2} \quad (5)$$

The bridging force (P) along the pulled-out part of the fiber can be resolved to a normal component (P_n) and a tangential component (P_t), as shown in Fig. 1(c). The force P_n and P_t can be considered as the bridging force for resisting crack opening and sliding, respectively, and are expressed as:

$$P_n = P \cos \gamma \quad (6)$$

$$P_t = P \sin \gamma \quad (7)$$

Due to the rotating of the fiber, the snubbing effect on the pullout behavior of single fiber is changed. In Eq. 3, the expression of snubbing effect is a function of ϕ , however, sliding has resulted in a change of the angle between the embedded and pulled out parts of fiber. To correctly describe the snubbing effect of single fiber behavior under combined opening and sliding, the expression should be modified as

$$P(\alpha) = P(0)g(\alpha) = P(0)e^{f\alpha} \quad (8)$$

The key to modeling the single fiber pullout behavior under combined opening and sliding is therefore to determine the intersection angle α . More generally, a 3D randomly oriented fiber bridging the crack is taken into account as shown in Fig. 2. Taking the intersection of the fiber and upper crack plane as the origin, a Cartesian coordinate η - μ - ξ is defined in Fig. 2, in which the plane μ - ξ represents the upper crack surface and η -axis is normal to the crack plane. The crack surfaces are assumed to slide along the direction of the μ -axis. To express the orientation of the embedded and pulled out components of the fiber bridging the crack, a spherical coordinate system is introduced, and the relation between the two coordinates is also depicted in Fig. 2. The orientation of the embedded part of the fiber is determined by arbitrary polar angle ϕ and azimuthal angle θ . After sliding, the relative geometric relationships among ϕ , θ , rotating angle γ and intersection angle α can be observed from Fig. 2. Based on the relative geometric relationships of the angles, the intersection angle α can be derived with trigonometric transform method and expressed as:

$$\alpha = \arccos(\cos \phi \cos \gamma + \sin \phi \sin \gamma \cos \theta) \quad (9)$$

In the case of 2D random distribution, the intersection angle α can be obtained by setting $\theta = 0$ in Eq. 9 to simplify the expression into:

$$\alpha = |\gamma - \phi| \quad (10)$$

2.3. Consideration of fiber strength reduction and rupture

For those fibers with strong slip-hardening behavior after fully debonded, Yang et al. [8] suggested that fibers with sufficiently long embedded length will rupture during the pullout process rather than being completely pulled out. In addition, some fibers are vulnerable to bending and shear, and consequently exhibit strength reduction effect when loaded at an inclined angle to the crack plane. This strength

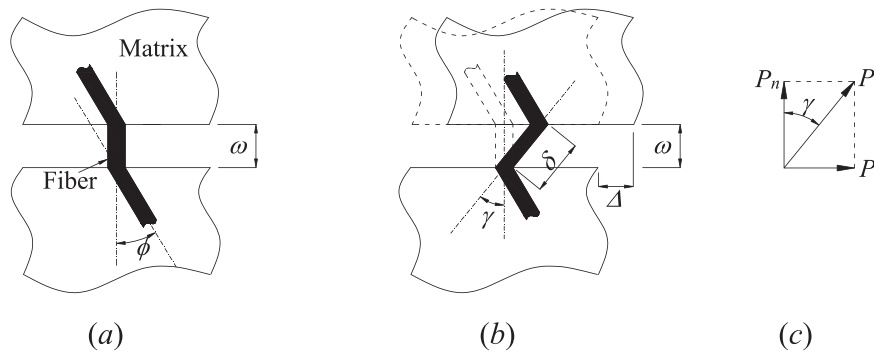


Fig. 1. A single fiber under (a) tension, (b) shear and (c) resolution of fiber force.

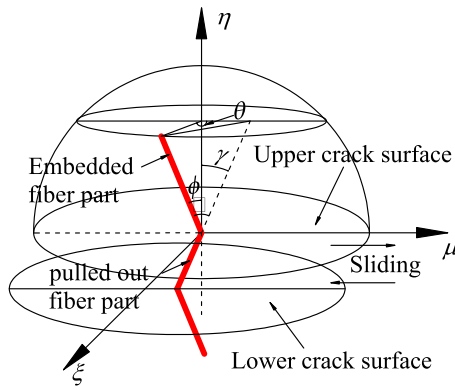


Fig. 2. The spatial position relation of the angles.

reduction effect was characterized with an exponential expression proposed by Kanda and Li [32] as follows:

$$\sigma_{fu}(\phi) = \sigma_{fu}(0)e^{-f\phi} \quad (11)$$

where σ_{fu} is the fiber rupture strength and f is the fiber strength reduction coefficient.

In this study, the same form is used except that the inclined angle ϕ is replaced by α . In the analysis procedure, fiber rupture will be considered when the calculated pullout force at an inclined angle ($P(\alpha)$) exceeds the rupture force ($P_{rp}(\alpha)$):

$$P(\alpha) > P_{rp}(\alpha) = P_{rp}(0)e^{-f'\alpha} \quad (12)$$

in which, $P_{rp}(0)$ is the rupture force of an aligned fiber, and $P_{rp}(0) = \sigma_{fu}(0)A_f$.

By substituting Eq. (8) into the inequality (12), it can be derived that a fiber will rupture if the following inequality is satisfied:

$$\frac{P(0)}{P_{rp}(0)} > e^{-(f'+f)\alpha} \quad (13)$$

2.4. Consideration of two-way debonding/pullout

For a fiber crossing a crack plane, the embedded fiber lengths on the two sides of the crack are generally different. If the bridged fiber does not exhibit slip hardening behavior in the pullout stage ($\beta \leq 0$), the fiber force will decrease with the increasing crack opening/sliding after the shorter embedded side of the fiber is completely debonded, and consequently the side with longer embedded length will never enter the pullout stage. In this case, we only need to consider one-way debonding. However, for fibers with slip hardening behavior in the pullout stage ($\beta > 0$), increase in applied force required for continued pullout of the shorter embedded side may result in full debonding and pullout of the longer embedded side.

The consideration of two-way debonding/pullout was first

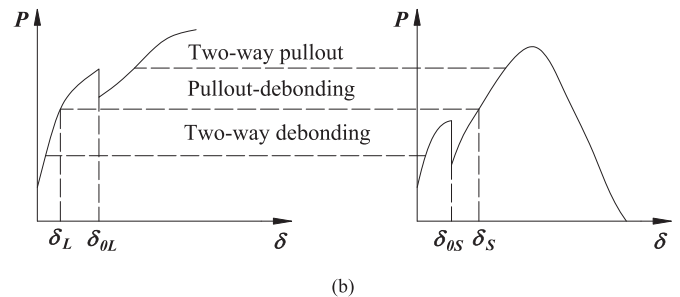
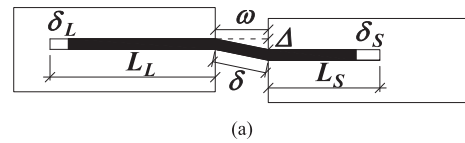


Fig. 3. Schematic diagram of two-way pullout consideration of a fiber: (a) diagram of two-way fiber pullout mechanism; (b) three balance conditions.

suggested by Wang et al. [33], and the modeling of two-way fiber debonding/pullout under pure crack opening was proposed in Yang et al. [8]. The modeling of two-way fiber debonding/pullout under the combined crack opening and sliding is illustrated in Fig. 3(a). At given ω and Δ of a single crack, the total actual pullout length δ can be determined by Eq. (5), and can be considered as the sum of pullout lengths in both sides and expressed as:

$$\delta = \delta_S + \delta_L \quad (14)$$

in which, δ_S and δ_L are the pullout length contributed from the sides with shorter embedded length (L_S) and longer embedded length (L_L) respectively.

As shown in Fig. 3(b), with the increase of δ , three possible conditions may be experienced before the fiber is ruptured or fully pulled out. As the fiber force acting on the two sides must be the same, δ_S and δ_L can be determined with the following equations corresponding to three different conditions [8,34].

(1) Two-way debonding:

$$\delta_L = \delta_S = \frac{1}{2}\delta, (\delta < 2\delta_{0S}) \quad (15)$$

(2) Pullout-debonding:

$$P_d(\delta_L, L_L) = P_p(\delta_S, L_S), (\delta_S > \delta_{0S}, \delta_L < \delta_{0L}) \quad (16)$$

(3) Two-way pullout:

$$P_p(\delta_L, L_L) = P_p(\delta_S, L_S), (\delta_S > \delta_{0S}, \delta_L > \delta_{0L}) \quad (17)$$

The debonding load P_d and pullout load P_p are given by Eq. 1(a) and Eq. 1(b), respectively. While δ_{0S} and δ_{0L} are the critical displacement

corresponding to complete debonding in the shorter and longer embedment side respectively, and can be determined with Eq. (2) by inputting corresponding embedded length as follows:

$$\begin{cases} \delta_{0S} = u_0(L_S) \\ \delta_{0L} = u_0(L_L) \end{cases} \quad (18)$$

2.5. Consideration of matrix micro-spalling

It is widely observed that matrix spalling would happen around the fiber exit point when the pullout force is at an angle to the embedded fiber segment [31,35,36]. The spalling of matrix usually leads to relaxation of the fiber and change of inclination angle, which can result in the delaying or prevention of fiber rupture; therefore, it could affect the fiber bridging behavior and should be considered. Kabele [27,28] assumed that matrix spalling occurs if the angle between the fiber embedment direction and relative crack displacement direction of a fiber (i.e. angle α in this study) exceeds a constant critical angle, and the fibers that may induce matrix spalling are not included in the calculation of total bridging force. However, the critical angle should not be constant [37], and even though the fiber is relaxed after spalling, it will become taut again on further displacement if the fiber is not ruptured. Based on the fiber pullout test result of PVA-ECC, Yang et al. [8] proposed a semi-empirical equation for estimating the spalling size, in which the spalling size is assumed to be proportional to the external load acting on the fiber exit point, and inversely proportional to matrix tensile strength and fiber diameter. This method is proposed for fibers under pure crack opening, in which the inclination angle cannot exceed $\pi/2$. However, for combined opening and sliding, which is the focus of this paper, the intersection angle α between the direction of embedded fiber segment and the pullout direction may theoretically vary from 0 to π . For this case, the applicability of the equation in Yang et al. (2008) needs to be further verified.

As a matter of fact, matrix spalling is governed by the component of reaction force acting perpendicular to the matrix at the exit point (R_{sp} in Fig. 4). R_{sp} can be calculated from the force balance as:

$$R_{sp} = P(\alpha) \sin \alpha \quad (19)$$

To model matrix spalling, Leung et al. [36] introduced an effective size of frictional pulley, L_r , over which R_{sp} is assumed to distribute around the exit point of the fiber. Spalling is assumed to occur if R_{sp} is larger than a spalling force F_s , which is obtained in the following manner. Using finite element analysis, Leung and Li [37] obtained the spalling force per unit length F_{sp} as a function of h/r_f , in which h is the distance between the bottom of the fiber and crack surface and r_f is the fiber radius (Fig. 5(a)). After being normalized by $r_f \sigma_m$, where σ_m is the effective spalling strength of matrix, the relationship between non-dimensional terms $F_{sp}/(r_f \sigma_m)$, and h/r_f is shown in Fig. 5(b). Such a relationship has been found to be insensitive to fiber/matrix modulus ratio in Leung and Li [37]. Since the distance along the fiber, x , can be

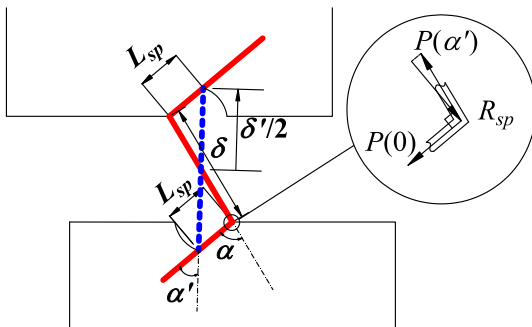


Fig. 4. Schematic diagram of matrix spalling for an inclined fiber under opening and sliding.

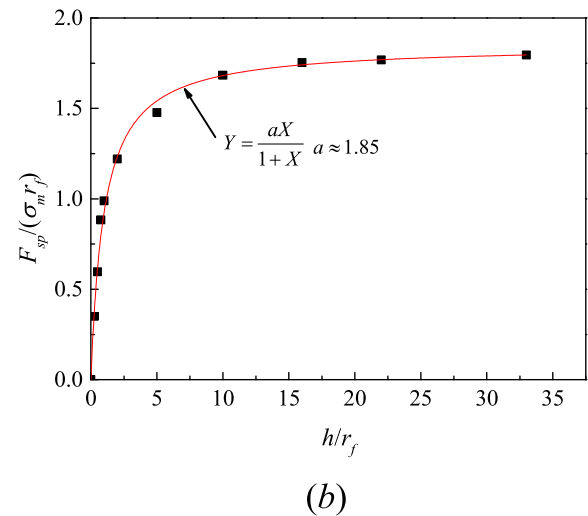
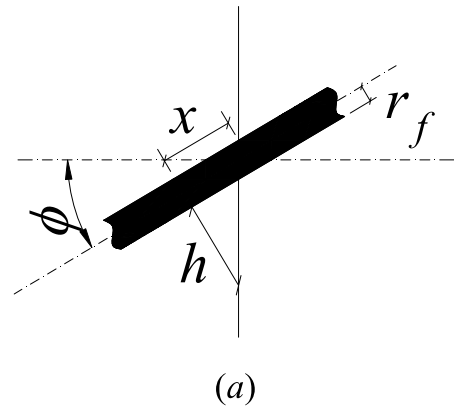


Fig. 5. Derivation of matrix spalling criterion in Leung et al. [36] (a) geometrical relationship between x and h ; (b) fitting of $F_{sp}/(r_f \sigma_m) - h/r_f$ relationship.

expressed, at any inclination angle ϕ , as $x = h \tan \phi$, the relationship between F_{sp} and x can be obtained. Assuming matrix spalling occurs at the same discrete length equal to L_r , the force required for the N th piece of matrix to spall, $F_s(N)$, can be obtained by integrating F_{sp} from $x = (N-1)L_r$ to NL_r .

This method is more precise and general and thus applied in this study. For simplification, the relationship between $F_{sp}/(r_f \sigma_m)$ and h/r_f obtained numerically in Leung and Li [37] is fitted by a closed form equation, which can provide good agreement with numerical data:

$$Y = \frac{aX}{1 + X}, \quad a \approx 1.85 \quad (20)$$

By substituting $Y = \frac{F_{sp}}{\sigma_m d_f / 2}$ and $X = \frac{h}{d_f / 2} = \frac{x \cot \phi}{d_f / 2}$ into the equation above, the spalling force per unit length F_{sp} can be expressed as:

$$F_{sp}(x) = \frac{ad_f \sigma_m x \cot \phi}{d_f + 2x \cot \phi} \quad (21)$$

The spalling force F_s required at any spalling size x_{sp} can be obtained by integrating F_{sp} from 0 to x_{sp} which gives the following equation:

$$F_s(x_{sp}) = \frac{1}{2} ad_f \sigma_m x_{sp} - \frac{1}{4} ad_f^2 \sigma_m \tan \phi \ln \left(1 + \frac{2x_{sp} \cot \phi}{d_f} \right) \quad (22)$$

In Eq. (22), the effective spalling strength σ_m is an empirical parameter that needs to be obtained through data fitting.

Unlike the method proposed in Leung et al. [36], the spalling process is considered to be “continuous”, and thus the matrix spalling size, L_{sp} , under certain R_{sp} can be obtained by solving the following equation:

$$R_{sp} = \frac{1}{2}ad_f k\sigma_t L_{sp} - \frac{1}{4}ad_f^2 k\sigma_t \tan \phi \ln \left(1 + \frac{2L_{sp} \cot \phi}{d_f} \right) \quad (23)$$

In Eq. (23), a spalling coefficient, $k = \sigma_m/\sigma_t$ is introduced, in which σ_t is the tensile strength of matrix. By setting the parameter k to be 1500, the calculated spalling length is approximately in the same range as the size of spalling in PVA-ECC specimens reported in Yang et al. [8]. This value of k is hence employed in the simulations of this study.

As mentioned above, spalling relieves the fiber stress and changes the fiber inclination angle α to a smaller angle α' (Fig. 4). For modeling the spalling effect in fiber bridging under pullout or crack opening, Leung et al. [36] and Yang et al. [8] derived the altered inclination angle and modified amount of pulling focusing on the one-way and two-way pullout respectively. Similarly, in this study, the altered inclination angle α' and modified amount of pulling δ_{eff} after spalling can be obtained with the following equations:

$$\delta' = \sqrt{4L_{sp}^2 + 4\delta L_{sp} \cos \alpha + \delta^2} \quad (24)$$

$$\alpha' = \arccos \left(\frac{4L_{sp}^2 + \delta'^2 - \delta^2}{4\delta L_{sp}} \right) \quad (25)$$

$$\delta_{eff} = \delta' - 2L_{sp} \geq 0 \quad (26)$$

It should be noted that since the range of α is from 0 to π , arccosine function is applied instead of arcsine function in Eq. (25). After spalling, the angle α in Eq. (19) and δ in Eq. (14) should be replaced by the altered inclination angle α' and modified amount of pulling δ_{eff} respectively. It should be noted that when angle ϕ approaches $\pi/2$, matrix spalling will occur easily even under a low R_{sp} and the spalling size may be infinite large. In practice, the spalling size cannot exceed the fiber embedment length L_e , therefore when the calculated $L_{sp} > L_e$, the related fiber force is reduced to zero and not included in the total bridging force. In some case, the calculated L_{sp} may be larger than $\delta'/2$, and leads to $\delta_{eff} < 0$. In this case, the fiber is usually no longer in tension and likely to buckle, therefore, the fiber cannot contribute to the total bridging force and the related fiber force is also considered as zero when $\delta_{eff} < 0$.

Another special phenomenon that should be noticed is that when a single bridged crack is under pure crack opening, matrix spalling can occur theoretically for fibers with any inclined angle if the load acting on the fiber exit point is high enough and the fiber has not ruptured. However, when a single bridged crack is under combined opening and sliding, spalling may never occur for fibers with α within a certain range. Taking 2D fiber distribution as an example, Fig. 6 shows a fiber with various inclined angles pulled along a certain direction. The embedded fiber segment divides the matrix around the fiber into two parts. The part with acute angle between the embedded fiber segment and crack plane is defined as “weak side”, while the other part is defined as “strong side” (as shown in Fig. 6(a)). It is obvious that spalling will always occur at the weak side of the matrix. Specifically, for a fiber bridging a crack under pure opening, for any inclined angle, the force component acting perpendicular to the embedded fiber segment P_{sp} will lead to matrix spalling near the fiber exit point at the weak side if P_{sp} is high enough (as shown in Fig. 6(a) and (b)). For a bridged fiber under

combined opening and sliding, in the condition shown in Fig. 6(c) and (e), P_{sp} acts towards the matrix at the weak side and thus spalling will occur when P_{sp} exceeds a critical spalling force. However, for the situation illustrated in Fig. 6(d), the P_{sp} acts towards the strong side of the matrix and spalling will never occur. Therefore, in the case of 2D opening and sliding, spalling will not occur when $0 \leq \phi \leq \gamma$ ($\phi \in [-\pi/2, \pi/2]$), otherwise, matrix may spall when the spalling criterion is satisfied. Similarly, for 3D opening and sliding, it is derived that spalling will never occur when the following inequality is satisfied:

$$\sin \phi \cos \gamma - \cos \phi \sin \gamma \cos \theta \leq 0 \quad (27)$$

Therefore, in the numerical procedure of the proposed model, the spalling criterion will not be checked if the inequality (27) is satisfied.

3. Shear/normal bridging stress-crack opening/sliding relations

With the equations derived above, the single fiber behavior under combined opening and sliding can be completely modeled. However, in the fiber composite, a single crack is bridged by numerous fibers with various locations and orientations. Due to the randomness of fiber location and orientation, the crack bridging stress-crack opening/sliding relation can only be obtained statistically. Li et al. [29] proposed a method for modeling the composite crack bridging stress-crack opening relation by averaging the contribution of all fibers crossing the crack plane at any possible location (along its length) and orientation. This method is also applied in this study, and the averaged crack bridging shear stress (τ_b), considering the randomness of fiber distribution, can be obtained by the following integral form:

$$\tau_b(\omega, \Delta) = \frac{V_f}{A_f} \int P_t(\delta, z)g(\alpha)p(z)p(\phi)p(\theta)dzd\phi d\theta \quad (28)$$

where, V_f and A_f are respectively the fiber volume fraction and cross-section area. z is the distance from fiber centroid to the crack plane, and $z = (L_f/2 - L_e)\cos\phi$. $P_t(\delta, z)$ is the shear bridging force contributed by a single fiber with a certain pullout displacement and centroidal distance z , and can be calculated from $P_t = P\sin\gamma$, where P is the force along the pulled-out part of the fiber. Function $p(z)$, $p(\phi)$ and $p(\theta)$ are the probability density functions of z , ϕ and θ , respectively. It should be noted that the integral for obtaining crack bridging stress-crack opening relation in Lin et al. [25] and Yang et al. [8] does not include the angle θ , but in this study, orientation angle θ should be included as 3D random distribution of the fibers is considered. In the case of uniform random distribution of fibers, the probability density functions are given by the following expressions:

$$p(z) = \frac{2}{L_f}, z \in \left[0, \frac{L_f}{2} \right] \quad (29)$$

$$p(\phi) = \begin{cases} \frac{1}{\pi}, \phi \in \left[-\frac{\pi}{2}, \frac{\pi}{2} \right] & \text{for 2D} \\ \sin \phi, \phi \in \left[0, \frac{\pi}{2} \right] & \text{for 3D} \end{cases} \quad (30)$$

$$p(\theta) = \frac{1}{2\pi}, \theta \in [0, 2\pi] \quad (31)$$

In general, when the fiber is fully 3D randomly distributed, Eq. 28

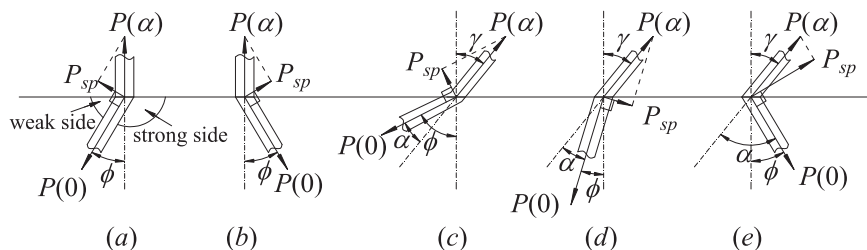


Fig. 6. Possible conditions for a fiber under opening or combined opening and sliding.

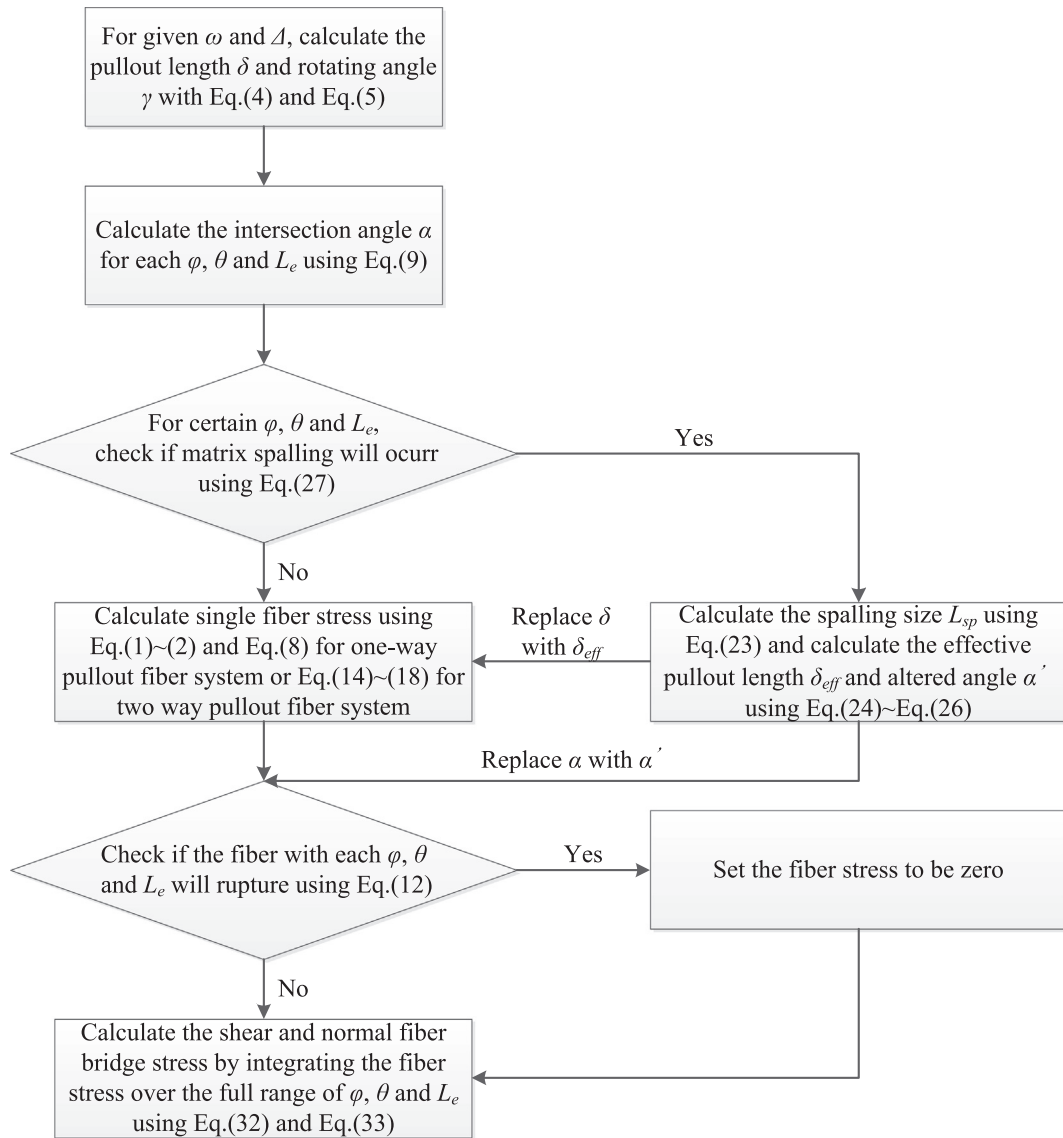


Fig. 7. Flow chart of the numerical procedure.

can be further expressed as:

$$\tau_b(\omega, \Delta) = \frac{V_f \sin \gamma}{A_f} \int_{\phi=0}^{\pi/2} \int_{z=0}^{(L_f/2) \cos \phi} \int_{\theta=0}^{2\pi} P(\delta, z)g(\alpha)p(z)p(\phi)p(\theta)dzd\phi d\theta \quad (32)$$

Similarly, the averaged crack bridging normal stress (σ_b) can be expressed as:

$$\sigma_b(\omega, \Delta) = \frac{V_f \cos \gamma}{A_f} \int_{\phi=0}^{\pi/2} \int_{z=0}^{(L_f/2) \cos \phi} \int_{\theta=0}^{2\pi} P(\delta, z)g(\alpha)p(z)p(\phi)p(\theta)dzd\phi d\theta \quad (33)$$

Since the analytic solution for the integrals in Eq. (32) and Eq. (33) is very difficult to obtain when considering all the micro-mechanisms discussed in Section 2, numerical computation is hence employed. The flow chart of the numerical procedure for computing the composite crack bridging shear/normal stress-crack opening/sliding relation is shown in Fig. 7. It should be noted that, for simplicity, Cook-Gordon effect [38] is neglected in this study. By coding with Matlab, a 3D curved surface of $\tau_b(\omega, \Delta)$ is generated and plotted in Fig. 8. The values of the micromechanics parameters used in this model are listed in Table 1, which are based on the related model inputs in Yang et al. [8].

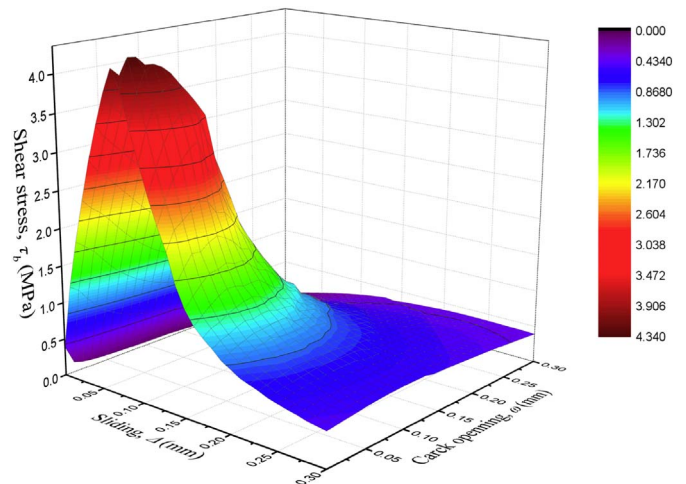


Fig. 8. The 3D curved surface of $\tau_b(\omega, \Delta)$ with the proposed model.

Table 1
Input value of micromechanics parameters used in proposed model.

Fiber parameters				Interface parameters				Matrix parameters				
d_f	σ_{fu}	V_f	τ_0	G_d	β	f	f'	E_m	σ_m	k		
/μm	/MPa	%	/MPa	/J/m ²				/GPa	/MPa			
39	1060	2	1.31	1.08	0.58	0.2	0.33	20	5	1500		

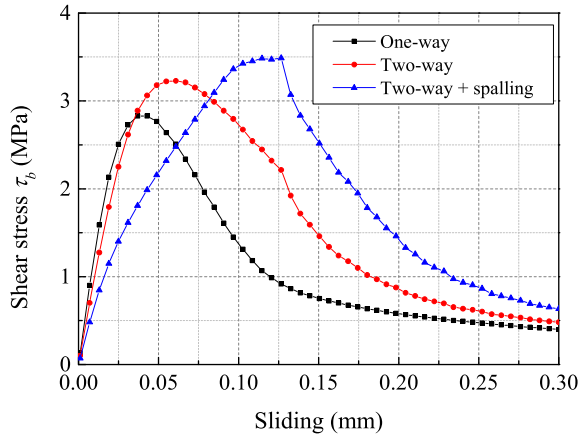


Fig. 9. Shear bridging stress-sliding curves with COD of 0.03 mm using various models.

The comparison of τ_b - Δ curves calculated by the models with one-way pullout, two-way pullout consideration and two-way pullout plus matrix spalling, respectively, are shown in Fig. 9. When using the model with one-way pullout mechanism, the predicted maximum shear stress that can be transferred through a fiber bridged crack is about 2.8 MPa, and its sliding displacement corresponding to the peak shear stress is about 40 μm. If two-way pullout mechanism is modeled but without considering matrix spalling effect, the calculated peak stress and its related sliding displacement are about 3.2 MPa and 60 μm, respectively. By using the model considering both two-way pullout and matrix spalling, the calculated peak stress and its related sliding displacement are about 3.5 MPa and 120 μm, respectively. It can be easily observed that both the peak stress and its corresponded sliding displacement predicted by the model considering two-way pullout are higher than those calculated by model considering only one-way pullout. Comparing the predicted results, if matrix spalling is considered, the slope of ascending branch of the calculated τ_b - Δ curve is lower, but both peak stress and its related sliding displacement are higher. The reason is as follows. Matrix spalling always leads to relaxation of the related fiber, which reduces the bridging stress. Meanwhile, matrix spalling also

effectively reduces the intersection angle α and consequently delays the rupture of fibers, leading to a final increase of the peak bridging stress. When the crack is under pure opening, Yang et al. [8] indicates that the contribution of matrix spalling to crack opening is rather small, but in the case of a crack under combined opening and sliding presented in this paper, matrix spalling is found to significantly affect the τ_b - Δ relationship. It can be explained that when shear sliding occurred in a crack, fibers bridging the crack are more vulnerable to rupture, and therefore the contribution of matrix spalling to delay the fiber rupture may become an important factor affecting the τ_b - Δ relationship.

4. Shear transmission on crack surface due to fiber bridging

In order to analyze the behavior of cracked members under shear loading the shear transfer behavior of crack surface must be properly modeled. However, shear transfer in cracks is a complicated phenomenon that is difficult to measure. For ordinary reinforced concrete (RC) members, shear stresses are transferred in cracks by a combination of aggregate interlock in concrete and dowel action in reinforcement, and the cracked concrete carry very low tensile stress. In the case of fiber reinforced cementitious composites (FRCC), significant tensile stress normal to the crack surface and shear stress along the crack surface can both be carried due to the fiber bridging action. In addition, it has been reported [21] that the interlock of fine aggregates in FRCC also contributes to the shear transfer of cracks when the crack opening does not exceed half of the maximum aggregate size. In addition, the dowel action should also be considered for FRCC with steel rebars. Since ECC generally does not contain coarse aggregates, and the maximum aggregate size of fine aggregate is very small, the effect of aggregate interlock should be limited except at very small crack openings. The dowel action from steel rebar is a different research topic that should be investigated separately. This study will focus on developing a model for the fiber bridging action alone, while the aggregate interlock and dowel action are left for future investigations.

Applying the model developed above, two sets of curves for various COD, including shear bridging stress vs. sliding curves and bridging normal stress vs. sliding curves, are plotted in Fig. 10(a) and (b) respectively. In Fig. 10(a) and (b), each curve was obtained by calculating

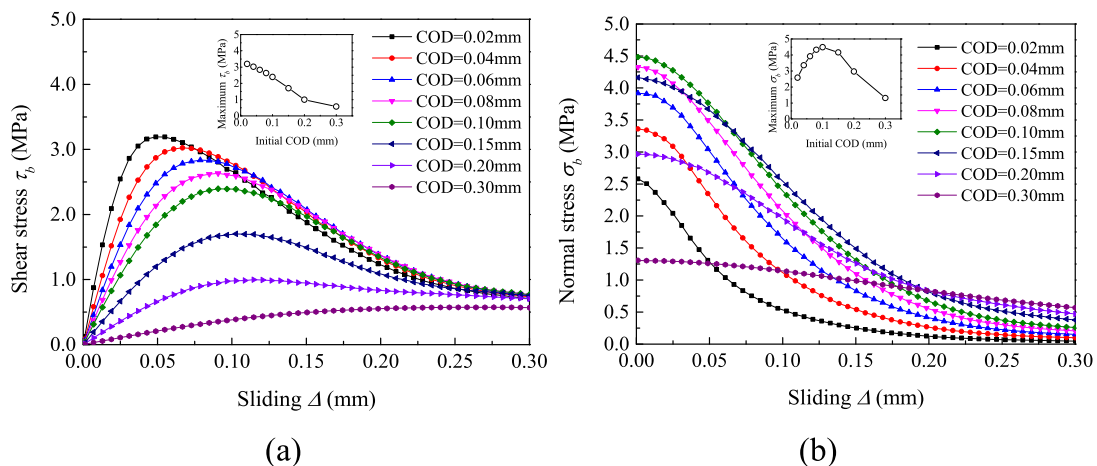


Fig. 10. Normal stress/shear stress-sliding curves with fixed COD.

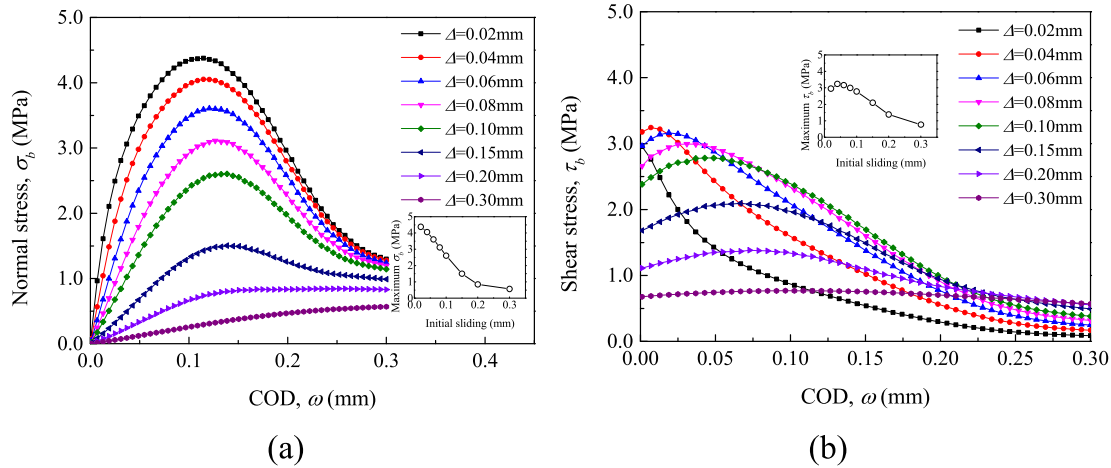


Fig. 11. Normal stress/shear stress-COD curves with fixed sliding.

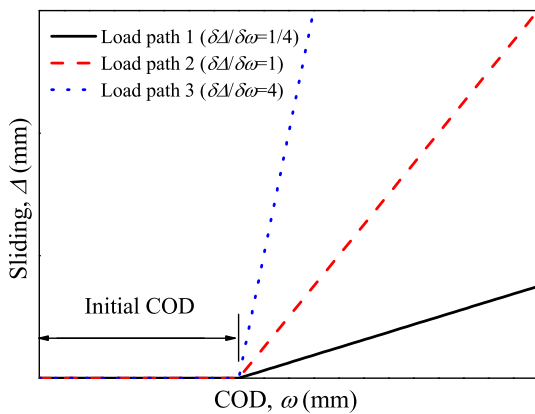


Fig. 12. Diagram of load path.

the stresses at fixed COD and increasing sliding displacement. It can be seen from the Fig. 10(a) that the peak shear stress decrease with increasing COD (as shown in the sub-figure in Fig. 10(a)), while the sliding displacements corresponding to the peak shear stresses increase. Moreover, larger COD leads to lower initial slopes of the shear stress-sliding curves, and the post-peak curves for relatively small COD first drop rapidly and then approach similar values at increasing sliding displacement. The physical explanation is as follows. When shearing is applied on the crack plane, the part of fiber between the crack faces is rotated to produce a tangential force component which increases initially with sliding distance as the rotated angle is increased. For the curves with small initial COD, most of the fibers are not pulled out or ruptured at the rising part. With increased sliding, fiber pull-out or rupture leads to the drop in stress after the peak. When the initial COD is large, a larger number of fibers crossing the crack plane have already been pulled out or ruptured before shear sliding was applied, and nearly 15% fibers pulled out or ruptured when the shear stress on the crack reaches the peak, after which the percentage of pulled-out/ruptured fibers kept increasing and the bridging shear stress started to decrease. However, for the case with COD = 0.2 (very large initial COD), about 77% fibers have already been pulled out or ruptured before shear sliding was applied, while at the peak shear stress the pulled out or ruptured fibers account for 83% of the total number. Fig. 10(b) shows that the normal stresses in all curves exhibit a downward trend with the increasing sliding displacement, and with increasing initial

COD, the peak normal stresses (also the initial stresses without shear sliding) increase at first and decrease afterwards, which follows the curve of bridging stress-COD of a single crack under pure opening (as shown in the sub-figure in Fig. 10(b)). The following reasons account for the decline of the normal stresses with growing sliding displacement. In this analysis, COD corresponding to each curve is fixed, while the sliding displacement increase, and hence the rotated angle γ of each fiber segment bridged between the two crack surfaces will increase. It is clear that the force component normal to the crack plane is the product of fiber pullout force and $\cos\gamma$. On one hand, $\cos\gamma$ is a decreasing function when γ vary from 0 to $\pi/2$; on the other hand, although the total pullout length of fibers δ will increase with rising sliding displacement, the growing γ leads to larger α for parts of the fibers, which may cause more severe fiber rupture (due to fiber strength reduction effect) or matrix spalling, and consequently the total fiber force along the pullout direction may reduce more rapidly. Taking the curve with COD = 0.06 as an example, when sliding displacement increases from 0 to 0.013, γ varies from 0 to 0.217 and $\cos\gamma$ decrease from about 1 to 0.98. Although the total fiber force per unit area along the pullout direction increases from 4.47 N/mm² to 4.39 N/mm², the normal stress still decrease from 4.47 MPa to 4.29 MPa. In addition, the percentage of pulled-out/ruptured fibers increases from 16% to 19%, which also retards the increase of total fiber force.

By fixing the sliding displacement and increasing COD, Fig. 11(a) and (b) show bridging shear stress vs. COD curves and bridging normal stress vs. COD, respectively. The characteristic shown in Fig. 11(a) is fairly similar to that of Fig. 10(a). However, different from Fig. 10(b), shear stress vs. COD curves in Fig. 11(b) does not just exhibit a downward trend. Instead, the curves are usually rising at first and decrease after reaching their peaks. In this case, since the sliding displacement is fixed for each curve, increasing COD will lead to the decrease of rotated angle γ ; meanwhile, the force component tangent to the crack plane is the product of fiber pullout force and $\sin\gamma$. Although the value of $\sin\gamma$ decreases with decreasing γ , the total pullout length of fibers δ increases with rising COD and may lead to increasing pullout force. Moreover, the declining γ may restrain fiber rupture or matrix spalling due to the decrease of α . Hence the shear stress vs. COD curves may contain an ascending branch.

In reality, sliding between two crack surfaces can only occur after the crack has been formed, therefore, a COD should be present before sliding starts. Assuming that a crack with an initial COD of 0.01 mm is under proportional loading, i.e. the increment ratio of sliding displacement to COD ($\delta\Delta/\delta\omega$) is constant, three loading paths with $\delta\Delta/\delta\omega$ equals to 0.25, 1 and 4 respectively are considered in this study as shown in Fig. 12. The responses under these three loading paths are shown in Fig. 13. It can be seen that the maximum normal stress of the

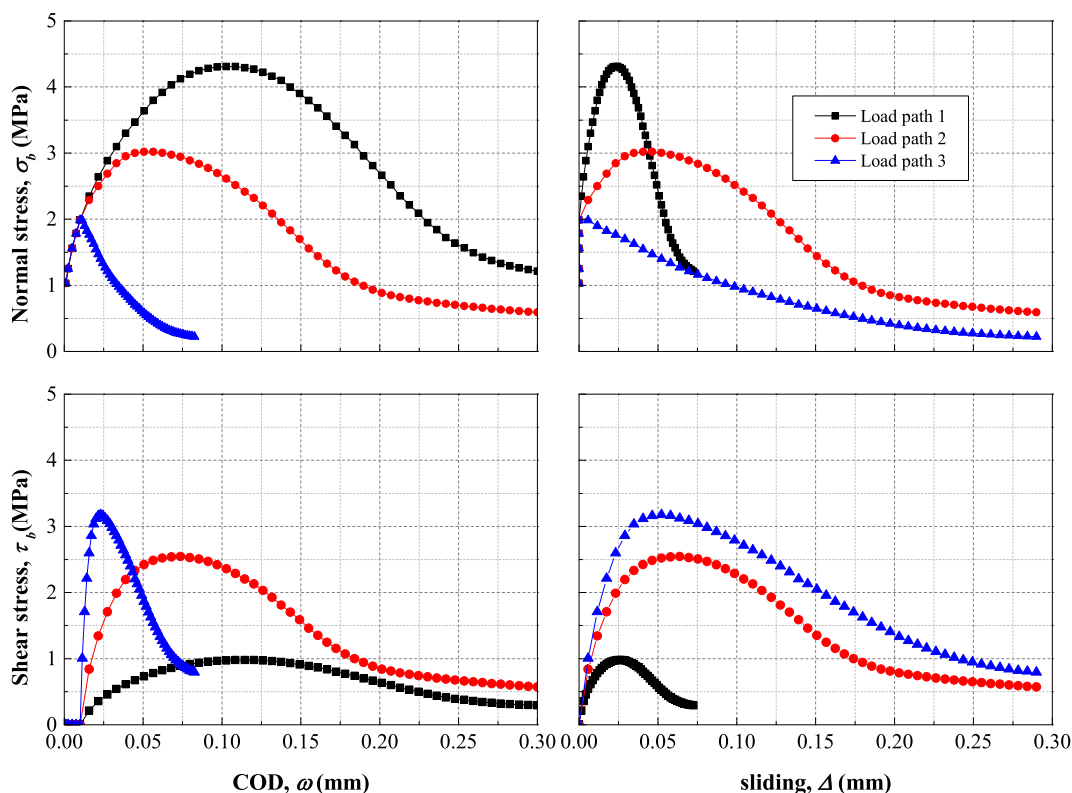


Fig. 13. Normal stress/shear stress-sliding/COD curves with proportional loading.

crack under load path 1 is the highest while its peak shear stress value is the lowest since the COD is always larger than sliding displacement and the COD will mainly govern the pullout behavior. On the contrary, the crack under load path 3 can transfer the highest shear stress, but the maximum normal stress is the lowest. And it can also be seen that the normal stress decreases consistently with increasing sliding displacement for the crack under load path 3. For the crack under load path 2, although the increments of sliding displacement and COD are the same, the value of peak shear stress (about 2.5 MPa) is slightly lower than that of peak normal stress (about 3 MPa) due to the presence of initial COD.

5. Effect of micromechanical parameters

The fiber bridging behavior of a crack is significantly influenced by the properties of fiber, matrix and especially their interface, which can be quantified by different micromechanical parameters. Since the derivation of the model is based on micromechanics, the effect of various micromechanical parameters can be investigated to provide insights on material design to improve the shear behavior. In this study, three micromechanical parameters: fiber length L_f , slip-hardening coefficient β and snubbing coefficient f , are considered to analyze their effects on the fiber bridging behavior of a single crack in a cementitious composite.

The selection of fiber, mainly fiber type, content, length, etc., has a large influence on the performance of the fiber composite. Different types of fibers usually result in different mechanical properties of the composite and generate different fiber/matrix interfacial properties which will also affect the mechanical behaviors. In terms of fiber content, it can be easily observed in Eqs. (32) and (33) that the bridging stresses are linearly proportional to the fiber volume fraction V_f . However, in practice, excessively high V_f may lead to workability problems which cannot be accounted for in the proposed model. Fig. 14(a) shows the effect of fiber length on the response curve of shear bridging stress vs. sliding displacement. It can be seen from Fig. 14(a) that the peak shear stress increases with the increase of fiber length

when initial COD is 0.03 mm; conversely, τ_b - Δ curve with shorter fiber length has higher peak shear stress with larger initial COD of 0.06 mm. This is because although the bridging stress is higher with longer fibers, fiber rupture is also easier to occur with increasing fiber length. When the COD is small, there is limited fiber rupture so longer fibers give better results. When the COD is large, longer fibers are easily ruptured so shorter fibers are preferable.

Besides the properties of the fiber itself, the property of fiber/matrix interface is also a governing factor to the crack bridging behavior. The slip-hardening coefficient β controls the pullout behavior of a single fiber embedded in a matrix after the fiber is completely debonded. Fig. 14(b) plots the τ_b - Δ curves with different values of β ($\beta = 0.58$, $\beta = 0$ and $\beta = -0.58$). It is demonstrated in the figure that the peak stress in the τ_b - Δ curve for $\beta = 0.58$ is larger than other cases. Interestingly, although the peak stress with $\beta = 0$ is lower than that with $\beta = 0.58$, the decreasing rate of the post peak branch in the τ_b - Δ curve with $\beta = 0$ is much lower. The physical explanations are as follows. According to Eq. 14, the bridged fibers exhibit slip hardening behavior in the pullout stage when $\beta > 0$, slip softening when $\beta < 0$, and linear slip softening when $\beta = 0$ (as shown in the sub-figure in Fig. 14(b)). For fibers that exhibit slip hardening behavior, more and more fibers will be ruptured with the increase of crack opening and sliding. In contrast, for those fibers with slip softening behavior, fiber will not rupture after the fiber is completely debonded since the fiber force will decrease in the pullout stage, and thus fibers can be fully pulled out theoretically if the chemical bond between the fiber and matrix is not high. When $\beta = 0$, the P - u relationship in the pullout stage decreases in a linear manner while the pullout force for $\beta < 0$ shows the trend of a concave parabola, and may decrease rapidly to low values. Therefore, post-peak τ_b - Δ curve is steeper for $\beta < 0$ than that for $\beta = 0$. The snubbing coefficient f also significantly affects the amount of fibers that will rupture. Theoretically, higher value of f renders fibers more vulnerable to rupture. This is well reflected in Fig. 14(c), in which, the τ_b - Δ curves show decrease of shear bridging stress with the increase of f . In addition, the interfacial friction factor τ_0 is also an important effect factor on the

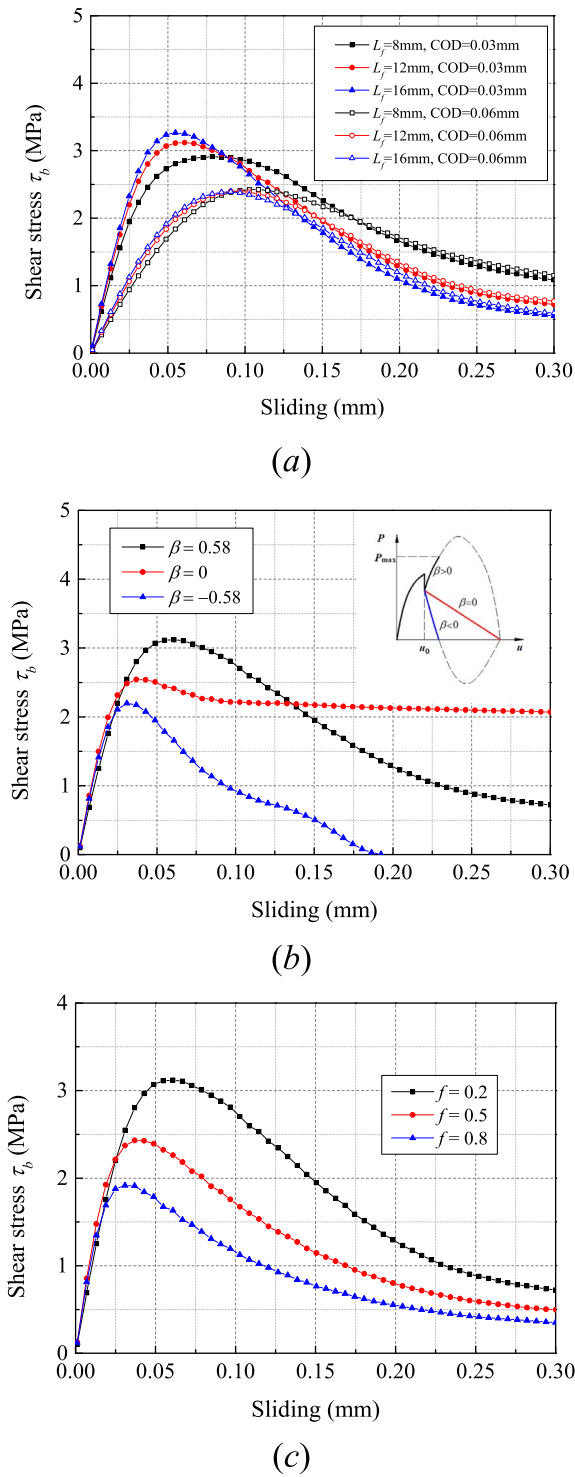


Fig. 14. Effect of micromechanical parameters on shear stress-sliding relation: (a) Effect of L_f ; (b) Effect of β ; (c) Effect of f .

Table 2
The applicability of proposed model.

Fiber type	Representative fiber	Applicability
Brittle fiber with low stiffness and high rupture strain	Low modulus PP fiber	Model without considering fiber rupture and matrix spalling
Brittle fiber with relatively high stiffness and low rupture strain	PVA fiber	Model considering fiber rupture and matrix spalling
Fiber with slip softening behavior at pullout stage	PP fiber	Model considering one-way pullout
Fiber with slip hardening behavior at pullout stage	PVA fiber	Model considering two-way pullout
Ductile fiber	Steel fiber	Unusable

fiber bridging behavior of a crack. The effect of τ_0 has been analyzed by the authors, and is found to be qualitatively similar to the effect of β (i.e., a higher leads to higher peak stress but more rapid post-peak drop due to increasing fiber rupture). Due to the similarity, detailed results are not shown in this paper.

6. Discussion of the applicability for the proposed model

In the present model, fibers are assumed to be perfectly flexible (with zero flexural stiffness), and thus fibers will act like string and snubbing friction model is used. Theoretically speaking, the snubbing mechanism can rationally represent the behavior of flexible fibers (low modulus and/or small diameter for low bending stiffness, and high rupture strain), and is not perfectly suitable for fibers with high stiffness or ductile yielding behavior [4]. It should be noted that the PVA or PE fibers employed for making ECC are very small in size. Therefore, even though the modulus of these fibers is higher than that of concrete, the fiber can still be treated as a flexible element as long as the crack opening (and hence the “bent” part of the fiber) is not too small, so the snubbing model is applicable. It can also be noted that for fibers with slip softening behavior at pullout stage, one-way pullout model can be used in this model for simplicity without losing accuracy; while, for fibers with slip hardening behavior at pullout stage, mechanism of two-way pullout has to be considered.

The proposed model is unusable for ductile fibers, such as steel fibers, since the bending effect can not be neglected. To model those fibers that flexural stiffness are not negligible, Kabele [28] considered the bridged fiber component between the crack surfaces as a beam and derived an equation for calculating the shear force carried by a single fiber using Timoshenko beam theory.

The applicability of the proposed model is listed in Table 2.

7. Conclusions

In this study, bridging stresses, including normal stress and shear stress, on the crack surfaces of ECC under combined opening and shear sliding are derived via micromechanics and averaging technique. Specifically focusing on flexible fibers, the proposed model can be seen as an expansion of the fiber-bridging model developed by Yang et al. [8], which only covers the normal bridging stress vs. COD relationship. Due to the shear sliding between the crack surfaces, the snubbing effect, fiber strength reduction, fiber rupture and matrix spalling criteria are modified or redeveloped. Two-way fiber pullout mechanism is also considered in this study for fiber systems with slip hardening behavior at pullout stage, such as PVA-ECC system.

More importantly, the model provides a theoretical interpretation for the contribution of fiber bridging action on the shear transfer behavior of cracked ECC. By varying COD/sliding, the normal/shear bridging stress vs. COD/sliding curves are analyzed to investigate behavior of a single crack in ECC under mixed mode crack condition. To simulate the commonly occurred situation, the responses of a crack with initial COD under different proportional loadings are also analyzed. In addition, the effects of fiber length L_f , slip-hardening coefficient β and snubbing coefficient f on the shear transfer behavior on the crack surface of ECC are investigated through a parametric study. The

simulation results can provide insight on the behavior of ECC under shear loading when cracks are propagating under mixed mode and provide guidelines for selecting composite micro-parameters to improve the shear behavior of ECC. The model also provides fundamental information that can facilitate the development of a rational model for predicting the shear behavior of ECC members, which will be developed in the future.

Acknowledgement

This research did not receive any specific grant from funding agencies in the public, commercial, or not-for-profit sectors.

References

- [1] A.E. Naaman, High performance fiber reinforced cement composites, Proceedings of the IABSE Symposium on Concrete Structures for the Future, Paris, France, 1987, pp. 371–376.
- [2] A.E. Naaman, H.W. Reinhardt, Setting the stage: toward performance-based classification of FRC composites, in: A.E. Naaman, H.W. Reinhardt (Eds.), High Performance Fiber Reinforced Cement Composites (HPFRCC-4), Proceedings of the 4th Int'l RILEM Workshop, RILEM S.A.R.L., Ann Arbor, USA, 2003, pp. 1–4.
- [3] G. Chanvillard, S. Rigaud, Complete characterization of tensile properties of ductal UHPFRC according to the French recommendations, in: A.E. Naaman, H.W. Reinhardt (Eds.), High Performance Fiber Reinforced Cement Composites (HPFRCC-4), Proceedings of the 4th Int'l RILEM Workshop, RILEM S.A.R.L., Ann Arbor, USA, 2003, pp. 21–34.
- [4] V.C. Li, C.K. Leung, Steady-state and multiple cracking of short random fiber composites, *J. Eng. Mech.* 118 (1992) 2246–2264.
- [5] V.C. Li, H. Stang, H. Krenchel, Micromechanics of crack bridging in fiber reinforced concrete, *Mater. Struct.* 26 (1993) 486–494.
- [6] V.C. Li, Engineered cementitious composites—tailored composites through micro-mechanical modeling, in: N. Banthia, A. Bentur, A. Mufri (Eds.), Fiber-reinforced Concrete: Present and the Future, Canadian Society for Civil Engineering, Montreal, Canada, 1998, pp. 64–97.
- [7] V.C. Li, Engineered Cementitious Composite (ECC)—Material, Structure and Durability Performance, CRC Press, Boca Raton, FL, USA, 2007.
- [8] E.-H. Yang, S. Wang, Y. Yang, V.C. Li, Fiber-bridging constitutive law of engineered cementitious composites, *J. Adv. Concr. Technol.* 6 (2008) 181–193.
- [9] J. Zhang, C.K. Leung, Y. Gao, Simulation of crack propagation of fiber reinforced cementitious composite under direct tension, *Eng. Fract. Mech.* 78 (2011) 2439–2454.
- [10] M. Maruta, T. Kanda, S. Nagai, Y. Yamanoto, New high-rise RC structure using precast ECC coupling beam, *Concrete Journal*, 43 Japan Concrete Institute, 2005, pp. 18–26.
- [11] V.C. Li, D.K. Mishra, et al., On the shear behavior of engineered cementitious composites, *Adv. Cem. Based Mater.* 1 (1994) 142–149.
- [12] T. Kanda, S. Watanabe, V.C. Li, Application of pseudo strain-hardening cementitious composites to shear resistant structural elements, *Fracture Mechanics of Concrete Structures Proceedings FRAMCOS-3*, AEDIFICATIO Publishers, D-79104, Freiburg, Germany, 1998, pp. 1477–1490.
- [13] H. Fukuyama, Y. Matuzaki, et al., Structural performance of engineered cementitious composite elements, 6th ASCCS Int'l Conf. on Steel-Concrete Composite Structures, Los Angeles, 2000, pp. 969–976.
- [14] G. Parra-Montesinos, J.K. Wight, Seismic response of exterior RC column-to-steel beam connections, *J. Struct. Eng. ASCE* 126 (2000) 1113–1121.
- [15] V. Xoxa, Investigating the shear characteristics of high performance fiber reinforced concrete, Master Thesis, University of Toronto, Toronto, 2003.
- [16] K. Shimizu, T. Kanakubo, T. Kanda, S. Nagai, Shear behavior of steel reinforced PVA-ECC beams, 13th World Conference on Earthquake Engineering, Conference Proceedings DVD, Vancouver, B.C., Canada, 2004 Paper No. 704.
- [17] K. Kesner, S. Billington, Investigation of infill panels made from engineered cementitious composites for seismic strengthening and retrofit, *J. Struct. Eng.-ASCE* 131 (2005) 1712–1720.
- [18] P. Kabele, Fracture behavior of shear-critical reinforced HFRCC members, in: G. Fischer, V.C. Li (Eds.), Proc. on the 49th Int. RILEM Workshop on HPFRCC in Structural Applications, USA, 2006, pp. 383–392.
- [19] G.P.A.G. Van Zijl, Improved mechanical performance: shear behaviour of strain-hardening cement-based composites (SHCC), *Cem. Concr. Res.* 37 (2007) 1241–1247.
- [20] L.J. Hou, S. Xu, X.F. Zhang, et al., Shear behaviors of reinforced ultrahigh toughness cementitious composite slender beams with stirrups, *J. Mater. Civ. Eng.* 26 (2014) 466–475.
- [21] I. Paegele, G. Fischer, Phenomenological interpretation of the shear behavior of reinforced engineered cementitious composite beams, *Cem. Concr. Compos.* 73 (2016) 213–225.
- [22] B. Suryanto, K. Nagai, K. Maekawa, Modeling and analysis of shear-critical ECC members with anisotropic stress and strain fields, *J. Adv. Concr. Technol.* 8 (2010) 239–258.
- [23] S.L. Xu, L.J. Hou, X.F. Zhang, Shear behavior of reinforced ultrahigh toughness cementitious composite beams without transverse reinforcement, *Mater. Civ. Eng.-ASCE* 24 (2012) 1283–1294.
- [24] R. Zhang, K. Matsumoto, T. Hirata, et al., Shear behavior of polypropylene fiber reinforced ECC beams with varying shear reinforcement ratios, *J. JSCE* 2 (2014) 39–53.
- [25] Z. Lin, T. Kanda, V.C. Li, On interface property characterization and performance of fiber-reinforced cementitious, *J. Mech. Phys. Solids* 45 (1999) 763–787.
- [26] T. Kanakubo, K. Shimizu, S. Nagai, T. Kanda, Shear transmission on crack surface of ECC, Proceedings of FraMCoS-7, Jeju, Korea, 2010, pp. 1623–1630.
- [27] P. Kabele, New developments in analytical modeling of mechanical behavior of ECC, *J. Adv. Concr. Technol.* 1 (2003) 253–264.
- [28] P. Kabele, Multiscale framework for modeling of fracture in high performance fiber reinforced cementitious composites, *Eng. Fract. Mech.* 74 (2007) 194–209.
- [29] V.C. Li, Y. Wang, S. Backer, A micromechanical model of tension-softening and bridging toughening of short random fiber reinforced brittle matrix composites, *J. Mech. Phys. Solids* 39 (1991) 607–625.
- [30] J. Morton, G.W. Groves, The effect of metal wires on the fracture of a brittle-matrix composite, *J. Mater. Sci.* 11 (1976) 617–622.
- [31] V.C. Li, Y. Wang, S. Backer, Effect of inclining angle, bundling and surface treatment on synthetic fibre pull-out from a cement matrix, *Composites* 21 (1990) 132–140.
- [32] T. Kanda, V.C. Li, Interface property and apparent strength of high-strength hydrophilic fiber in cement matrix, *J. Mater. Civ. Eng.* 10 (1998) 5–13.
- [33] Y. Wang, V.C. Li, S. Backer, Modelling of fibre pull-out from a cement matrix, *Int. J. Cem. Compos. Light. Concr.* 10 (1988) 143–149.
- [34] C. Lu, C.K. Leung, V.C. Li, Numerical model on the stress field and multiple cracking behavior of engineered cementitious composites (ECC), *Constr. Build. Mater.* 133 (2017) 118–127.
- [35] J. Morton, G.W. Groves, The cracking of composites consisting of discontinuous ductile fibers in a brittle matrix-effect of fiber orientation, *J. Mater. Sci.* 9 (1974) 1436–1445.
- [36] C.K. Leung, N. Ybanez, Pullout of inclined flexible fiber in cementitious composite, *J. Eng. Mech.-ASCE* 123 (1997) 239–246.
- [37] C.K. Leung, V.C. Li, Effect of fiber inclination on crack bridging stress in brittle fiber reinforced brittle matrix composites, *J. Mech. Phys. Solids* 40 (1992) 1333–1362.
- [38] J. Cook, J.E. Gordon, C.C. Evans, D.M. Marsh, A mechanism for the control of crack propagation in all brittle systems, *Proc. R. Soc. London, Ser. A* 282 (1964) 508–520.